Circularly Polarized Coaxial Horn Filtenna for Electromagnetic Interference Mitigation

Steven Caicedo Mejillones, Matteo Oldoni, *Member, IEEE*, Stefano Moscato, *Student Member, IEEE*, Michele D'Amico, *Senior Member, IEEE*, and Gian Guido Gentili

***Abstract*— This article describes the design of a circularly polarized filtenna based on the insertion of radial stubs into a coaxial horn antenna. These stubs can be placed into the horn body or in the coaxial core, both cases are analyzed in this article. The radial stubs create transmission zeros (TZs) at their resonant frequency producing a stopband filter and preserving the polarization. This solution allows to integrate a filter function into the horn flare, so there is no need for additional space for the placement of an external filter. The gain of the filtenna in the passband is comparable with the gain of a standard horn with the same dimensions. For the chosen use case, the filtenna enables transmission to the ground of scientific data in the passband frequency range and minimizes interference with measurement equipment working in the stopband frequency range. A prototype has been manufactured and its measurements are in accordance with the simulations, validating the design principle.**

***Index Terms*— Circular horn, electromagnetic compatibility, filtering antenna, interference mitigation, space missions.**

I. Introduction

MANY of the anomalous occurrences in space systems are attributed to radio frequency disturbances generated in the same system, by third-party ones or by hostile surrounding environments affecting the on-board receivers [1]. The European Cooperation for Space Standardization (ECSS) has contributed in the years to develop a set of standards and handbooks to pursue all relevant aspects to space systems electromagnetic compatibility [2], [3], [4]. According to ECSS guidelines, the radio frequency interference between all the units of the space system shall be verified in the frame of the flight acceptance review (FAR), right before launch. In case any interference problem is found, a change in the position of the units is usually recommended, which is sometimes impractical. That is why this work proposes an innovative concept that may help to mitigate radio frequency interference on space systems. The proposed solution foresees the embedding of a stopband filter into a transmitting antenna to significantly mitigate its spurious emissions against a susceptible victim unit. A use-case is chosen to validate the proposed solution.

TABLE I
KA-BAND FILTENNA DESIGN TARGETS

Passband	25.5-27 GHz	RL $>$ 15 dB, Maximum gain $>$ 19 dBi, Axial Ratio (AR) $<$ 3.5 dB within HPBW.
Stopband	35.5-36 GHz	Minimum gain suppression $>$ 20 dB in all directions with respect to passband, desirable suppression $>$ 30 dB.

For the use-case, the filtenna has to meet the requirements described in Table I to enable transmission to the ground of scientific data in the portion of Ka-band reserved for communication with earth exploration and space research satellites [5]. The identified victim is a hypothetical onboard radiometer for improved sensing of snow and ice thickness [6] whose operating frequency corresponds to the filtenna stopband. The filtenna design must work with circular polarization and must be space-efficient, i.e., the stopband filter function must be integrated into the antenna as physical space is limited.

The antenna must operate in circular polarization, which is assumed to be carried by the feeding circular waveguide and externally generated by the waveguide launcher or suitable polarizers. To preserve the unitary axial ratio of such polarization, the antenna and its filtering structure will be designed to be axially symmetrical and therefore a circular conical horn will be used. Such symmetry guarantees that, although many higher modes can propagate thanks to the horn's flare, only those with azimuthal index $m = 1$ remain excited. The stopband will be generated by extracted-pole transmission zeros (TZs), which allow independent placement of each zero and can be implemented via axially-symmetrical radial stubs. Two options for the stubs are studied: 1) excavated in the horn antenna body and 2) the stubs carved into the metallic coaxial core. The latter allows having a standard horn as a base block and then inserting a suitable coaxial core according to the filter requirements. There have been some efforts to include a filter function into a horn antenna [7], [8], [9], [10], [11]. Compared to these works, the main advantage of the presented design is

Manuscript received 21 February 2023; revised 1 September 2023; accepted 11 September 2023. Date of publication 9 October 2023; date of current version 20 December 2023. This work was supported by the European Union's Horizon 2020 Research Program 5G STEP FWD under Grant 722429. *(Corresponding author: Matteo Oldoni.)*

Steven Caicedo Mejillones is with the Dipartimento di Elettronica, Informazione e Bioingegneria, Politecnico Di Milano, 20133 Milan, Italy, and also with the Research and Development Department, SIAE Microelettronica, 20093 Cologno Monzese, Italy (e-mail: stevenkleber.caicedo@polimi.it).

Matteo Oldoni, Michele D'Amico, and Gian Guido Gentili are with the Dipartimento di Elettronica, Informazione e Bioingegneria, Politecnico di Milano, 20133 Milan, Italy (e-mail: matteo.oldoni@polimi.it).

Stefano Moscato is with the Research and Development Department, SIAE Microelettronica, 20093 Cologno Monzese, Italy (e-mail: stefano.moscato@siaemic.com).

Color versions of one or more figures in this article are available at https://doi.org/10.1109/TAP.2023.3321422.

Digital Object Identifier 10.1109/TAP.2023.3321422

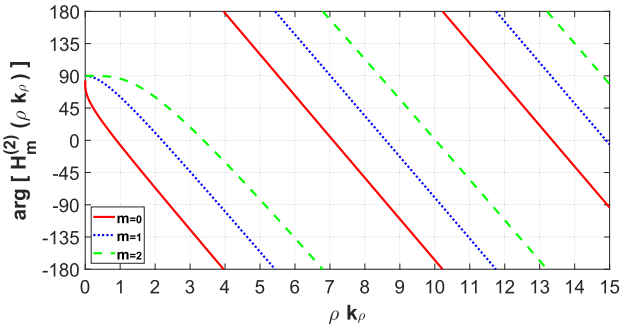

Fig. 1. Radial phase of cylindrical waves (1) for three azimuthal indices.

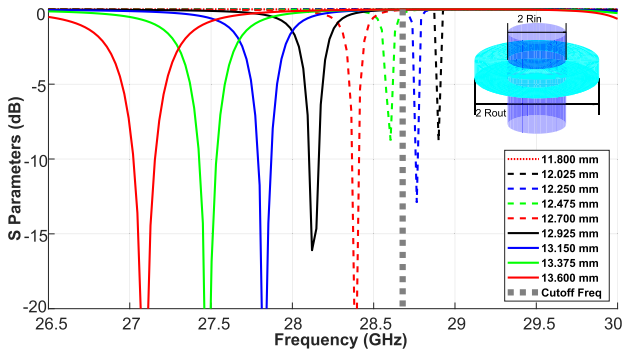

Fig. 2. $|S_{21}|$ through waveguide ($2R_{in}$ = 12.75 mm, cutoff TM_{11} : 28.7 GHz). Radial stub (height 2 mm, R_{out} ranging from 13.6 to 11.8 mm).

that the filtering structure is proven to support linear polarization, dual-linear, and circular polarization. The proposed work is an extension of our previously published papers [12], [13]. Unlike these past works, this one provides several additional insights into the filter design and moreover presents a novel design by leveraging stubs within the inner core, more easily manufacturable and applicable to existing horns. This article is organized as follows. Section II explains how the radial stubs work while Section III details the horn filtenna design principle. Then, Section IV focuses on the use-case design, and Sections V and VI deals with the manufacturing considerations and measurements, respectively. Sections VII and VIII show some alternative designs and a comparison with the other works. Finally, Section IX summarizes the conclusions.

II. Radial Stubs for Filtenna Design

Radial waveguides work by propagation of cylindrical waves from the central axis. The general scalar potential of cylindrical modes $C(\rho, \varphi, z)$ exhibits outward propagation along the radius ρ according to the Hankel function $H_m^{(2)}(x)$

$$C(\rho,\ \varphi,\ z) = H_m^{(2)}\left(k_\rho\,\rho\right)\ \sin(m\,\varphi)\,e^{j\,z\,k_z} \tag{1}$$

with $k_\rho^2 = \omega^2\,\mu\epsilon - k_z^2$ and $H_m^{(2)}(x) = J_m(x) - j\,Y_m(x)$, where m denotes the azimuthal index of the wave. By making these guides "thin," the fields can be considered constant along the longitude z ($k_z = 0$) and the radial phase is thus shown in Fig. 1, asymptotically linear. A short-circuited stub [14] resonates when its electrical length is $(N\,\pi)$ rad. The considered thin short-circuited radial stub hence resonates when the radial phase shown in Fig. 1 at the stub's radius $\rho = R_{out}$ differs by $(N\,\pi)$ rad from the radial phase when $\rho \to 0$, which tends to $(\pi/2)$ rad. This amounts to finding the values of $(k_\rho\,R_{out})$ where the radial phase is $(-(\pi/2) + N\,\pi)$ rad, which is equivalent to enforcing $J_m(k_\rho \cdot \rho) = 0$. The considered application assumes that only modes with azimuthal index $m = 1$ are present, as excited by the two degenerate TE_{11} fundamental modes composing the desired circular polarization in the feeding waveguide. The zeros $p_{m,n}$ of the Bessel function of first kind and order $m = 1$ are known [15]: $p_{1,1} = 3.832$, $p_{1,2} = 7.016$, $p_{1,3} = 10.174\ldots$. For a given radius R_{out}, the resonant angular frequencies ω_ρ can be found

$$\omega_\rho\,\sqrt{\mu\epsilon}\,R_{out} = p_{1,N}. \tag{2}$$

By choosing $R_{out} = 13.4$ mm, the $N = 2$ resonance is found for $\omega_\rho\,(\mu\epsilon)^{1/2}\,R_{out} = 7.0156$, as confirmed by Fig. 1. Please note that this coincides with the $N = 2$ root of $J_1(x) = 0$. The corresponding resonant frequency, in an air-filled stub, is found to be 24.9 GHz. Resonances of a radial stub coincide with the TM_{1N0} modes of a cylindrical cavity and with the TM_{1N} cutoff frequencies of a circular waveguide.

The above calculations refer to an unloaded stub. However, when the same radial stub is physically connected to a circular waveguide as shown in Fig. 2, the TZ is slightly affected: it occurs at 24.5 GHz when the feed waveguide has $\varnothing = 2\,R_{in} =$ 7.795 mm and at 27.46 GHz for $\varnothing = 12.95$ mm. This implies that after the theoretical design, a fine adjustment of the stubs is necessary to take into account the loading effect of the input and output lines.

Shrinking the stub radius increases the TZ frequency. However, a bound appears as shown in Fig. 2: the TZ becomes progressively narrower in terms of bandwidth and then, beyond the feed's TM_{11} cutoff, it gradually disappears. This phenomenon severely limits the application of the principle to a horn filtenna: a standard hollow horn exhibits a flare which makes the TM_{11} cutoff frequency significantly lower, transitioning toward the horn aperture. As a consequence, radial stubs would be forced to be located only in the narrow section, without exploiting the full length of the Horn.

As a countermeasure, a coaxial metal core can be introduced into the horn forming a coaxial line. Note that TE_{11} circular mode becomes TE_{11} coaxial mode. In a coaxial waveguide, the thinner the open annular ring, the higher the TM_{11} and the lower the TE_{11} frequency cutoffs, according to the corresponding transcendental equation [15] and as shown in Fig. 3. This degree of freedom is the key to overcoming the limits on the use of the stubs described above. In a coaxial waveguide, radial stubs can be initially designed by using the $m = 1$ curve in Fig. 1 so that the radial phase difference between the inner (R_{inStub}) and at outer radii ($R_{outStub}$) is $(N \cdot \pi)$ rad at the TZ frequency, equivalent to computing the coaxial TM_{1N0} resonant mode. Again, fine tuning of $R_{outStub}$ or R_{inStub} is required to take into account the interaction with the feed waveguide. Fig. 4 shows that the scattering response of such a stub corresponds to that of a transmission line loaded by a short-circuited transmission line section with characteristic impedance Z_{mode}: at the stub resonances ω_{mode}, a short circuit

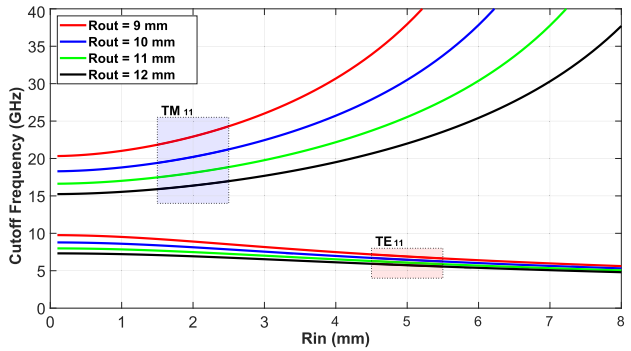

Fig. 3. Coaxial transmission line. TE_{11} and TM_{11} cutoff frequency for various inner (R_{in}) and outer radii (R_{out}).

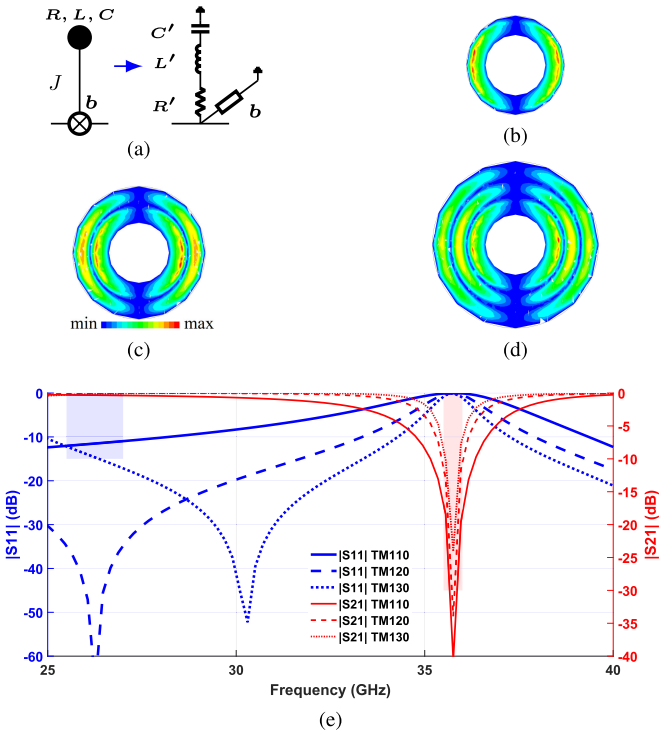

Fig. 4. Coaxial radial stubs and equivalent circuit. Dimensions of the input and output coaxial line are: $R_{in} = 7.5$ mm, $R_{out} = 11$ mm. Cut-off frequency of the TM_{11}: $F_{cutTM11} = 45$ GHz. Dimension of the stub: $R_{inStub} = R_{in}$. Resonant frequency $f_r = 35.75$ GHz. (a) Equivalent circuit for the coaxial radial stubs. For air—filled stubs, the losses are negligible, then $R' \approx 0$. (b) TM_{110}: $|\vec{E}|$ fields at f_r, $Z_{TM_{110}} = 4.6\ \Omega$, $R_{outStub} = 12.29$ mm. (c) TM_{120}: $|\vec{E}|$ fields at f_r, $Z_{TM_{120}} = 10.6\ \Omega$, $R_{outStub} = 16.54$ mm. (d) TM_{130}: $|\vec{E}|$ fields at f_r, $Z_{TM_{130}} = 17.5\ \Omega$, $R_{outStub} = 20.80$ mm. (e) Two-port scattering parameters of a coaxial transmission line loaded with radial stubs. The transparent rectangles highlight the limits of the passband (blue) and the stopband (red).

creates the TZ. This is approximated by lumped components as a shunt-connected series resonator $[b, R', L', C']$ or as a parallel resonator $[b, J, R, L, C]$ coupled by means of an admittance inverter J (also known as "extracted pole"). The frequency-independent susceptance b determines the location of the reflection zero. The resistance R' can be assumed 0 for low-loss devices such as air-filled horn antennas. The parameters in Fig 4(a) are related by

$$L' = \frac{C}{J^2}, \quad C' = L\,J^2, \quad w_r^2 = \frac{1}{L'C'}, \quad Z_c = \sqrt{\frac{L'}{C'}}. \tag{3}$$

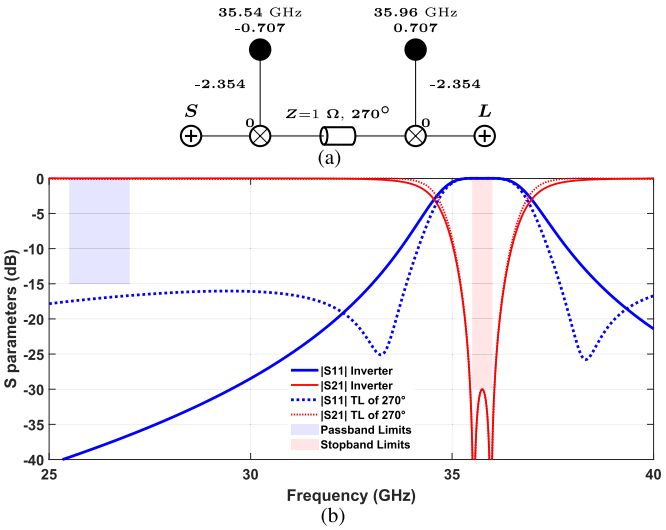

Fig. 5. Synthesized filtering function. $C = 1/(2\pi\,Bw)$. $L = 1/(\omega_r^2 C)$. Source S and load L are unitary impedance. (a) Synthesized stopband circuit. (b) Filter response with ideal coupling ("inverter") and 270° transmission line ("TL").

Fig. 4 shows that as N increases, the feed waveguide becomes less coupled to the resonant stub, therefore the bandwidth of its filtering function is reduced. In the equivalent circuit, this occurs when the characteristic impedance of the stub increases. Increasing N also moves the reflection zero closer to the TZ.

III. Design Principle

The previous section shows that coaxial radial stubs provide a simple yet powerful way to implement extracted poles. Following use-case specifications, we choose the stopband centered at 35.75 GHz with 600 MHz of bandwidth and 30 dB of attenuation, i.e., 100 MHz and 10 dB beyond the target.

A. Filter Synthesis

The first thing to do is to determine the minimum number of stubs required to fulfill the specifications. Then, we performed a synthesis of a first, second and third-order normalized all-pole Chebychev polynomials with 30 dB of return loss (RL) in the 35.5–36 GHz band. After, S_{11} and S_{21} polynomials were swapped to get the desired stopband behavior: the RL curve becomes the insertion loss (IL) one and vice-versa. This also implies that the reflection zeros become TZs. Then, the circuits are synthesized according to the method in [16] and, finally, they are denormalized in frequency.

According to the one-order circuit, the stub is required to have a characteristic impedance of 0.9 Ω or lower. As reported by Fig. 4, this is not even compatible with the TM_{110} coaxial mode which has the lowest impedance, i.e., $Z_{TM_{110}} = 4.6\ \Omega$.

Conversely, considering the third-order circuit, the stubs would need a characteristic impedance of 18 Ω, which is even compatible with the TM_{130} coaxial mode which has the highest impedance, i.e., $Z_{TM_{130}} = 17.5\ \Omega$. However, this mode has bad RL performance in the passband, i.e., ≈ 10 dB.

Instead, the second-order Chebychev filter shown in Fig. 5 requires only two stubs, each with characteristic impedance

of 10.5 Ω, practically coincident with the TM_{120} mode, i.e., $Z_{TM_{120}} = 10.6\ \Omega$, and with no degradation in the passband because its $|S_{11}|$ is lower than −30 dB.

The synthesis method produces a circuit with extracted poles connected by a constant phase shifter of 90° and constant impedance over frequency. To minimize cross-coupling between the subs, they are instead placed 270° apart. In order to have a more physical circuit, this ideal phase shifter is converted into a transmission line. The reference 270° phase shift is considered at the center of the stopband (f_{stop}) to preserve its behavior. Note that this inverter-to-transmission line conversion is exact at f_{stop} and less accurate away from it. Fig. 5 shows the ideal and the distributed response. A slight RL degradation is in fact visible in the passband, but always it is better than 15 dB.

B. Suitable Place for Filtering Function

Two potential problems have been identified for inserting the synthesized filtering function into the flare of a horn antenna. First, the excitation of the TM_{11} mode in the horn flare, which considerably reduces the filtering behavior of the stubs as explained above. Second, the synthesized filter prototype assumes a constant impedance for the transmission line connecting the stubs but the impedance of the horn changes gradually from its waveguide feeding to its aperture. However, due to the insertion of the coaxial core to mitigate the first potential issue, this impedance change can be abrupt, particularly in the vicinity of the circular-to-coaxial transition.

Therefore, for the implementation of the filter prototype in the horn to be as accurate as possible, the horn flare must have a suitable area that meets the following two conditions.

1) The TM_{11} cutoff frequency must remain "high" in order to allow the required stopband width of each stub while retaining an annular thickness sufficient to avoid high field concentration to contain losses.
2) The TE_{11} impedance should remain approximately constant between the two stubs in the stopband frequencies.

C. Design Procedure

The proposed design flow is therefore as follows.

1) Design a standard hollow circular horn to provide the required gain in the passband.
2) Design and insert a coaxial metal core such that as follows.
   a) The input section gradually transitions from the circular TE_{11} to the coaxial TE_{11} mode.
   b) The middle section must create a suitable annular opening to fulfill the two conditions described in the section above.
   c) The terminal part must narrow down up to the horn's mouth, for correct aperture illumination and same passband gain.
3) Insert the coaxial stubs in the middle section, dimensioning each one according to the resonance frequency and impedance given by the synthesized filter circuit. Here it must be chosen the TM_{1N0} mode that best suits the synthesized circuit.

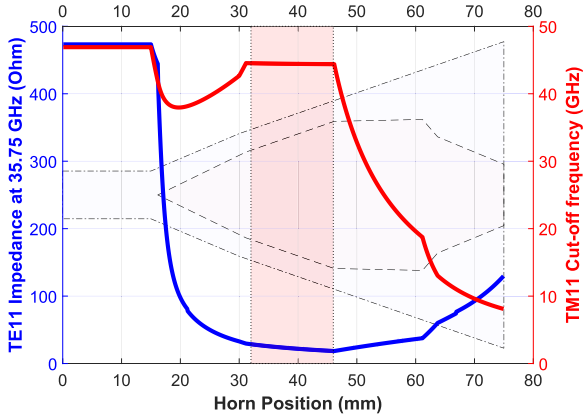

Fig. 6. Coaxial horn profile. The TE_{11} impedance along the coaxial horn at the center of the stopband is in blue. The TM_{11} cutoff along the coaxial horn is in red. In dotted-dashed lines is the standard horn profile (outer profile). In dashed lines is the coaxial core profile (inner profile). The suitable section for the stubs is highlighted in the dotted red rectangle.

IV. Use-Case Design

For the use case at hand, step 1 yields a circular horn with an aperture diameter of $\varnothing = 50$ mm and length of 65 mm for a 20 dBi antenna gain: the antenna is fed by a standard $\varnothing = 8.112$ mm circular waveguide.

Step 2 instead requires introducing and optimizing the coaxial core accordingly. This procedure is done by full-wave optimization. The obtained TE_{11} impedance and TM_{11} cutoff can be evaluated to identify a suitable region for the two stubs. This information is shown in Fig. 6 with the suitable region highlighted in red.

In step 3 finally, the two TM_{120} stubs have been dimensioned for the required resonance frequency and properly spaced at about 270° from each other, i.e., according to the filter prototype. Two options are provided for the stubs: as air sections expanding out of the body of the horn as shown in Fig. 7(a), or protruding into the body of the coaxial core like Fig. 7(b). Note that in the latter option, the horn profile remains standard and conversion to a filtenna is done just by inserting a suitable metal coaxial core designed according to the requirements of the filter function.

Fine-tuning may be necessary after the stubs are introduced in the design. The final designs are shown and detailed in Section IV-A.

A. Final Design and Simulation Results

The preliminary theoretical design of the proposed filtenna results in a manufacturable structure. The inner coaxial metal core filling the standard horn has been adjusted in its radial profile and is supported by two Teflon dielectric rings with a thickness equivalent to 180° of electrical length in the center of the passband, so the antenna matching is not affected by the rings. The two designs are detailed in Fig. 7. On the top, the stubs are placed in the horn profile (labeled as external stubs). On the bottom, the stubs are placed in the coaxial core profile (labeled as internal stubs). Simulated results are reported in Fig. 8, which shows the input matching and the broadside realized gain over frequency normalized to the value

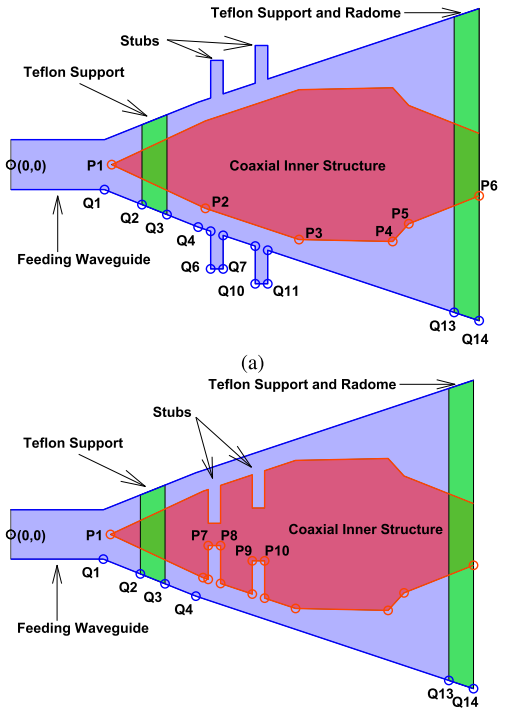

Fig. 7. Filtenna profile. Lateral view. Outer profile (blue) is piecewise linear and it is given in mm by $Q = [(0,4.17), (15,4.17), (21,6.4), (25,8), (30,10), (32,32/3), (32,16.7), (34,16.7), (34,34/3), (39.14,39.14/3), (39.14,19.083), (41.14,19.083), (41.14,41.14/3), (71,71/3), (75,25)]$. Inner profile (red) is piecewise linear and it is given in mm by: $P = [(16.155,0), (31.155,7), (46.155,12), (61.155,12.311), (63.734,9.473), (75,5), (32,1.81), (34,1.81), (39.14,4.28), (41.14,4.28)]$. (a) Horn filtenna with external stubs. (b) Horn filtenna with internal stubs.

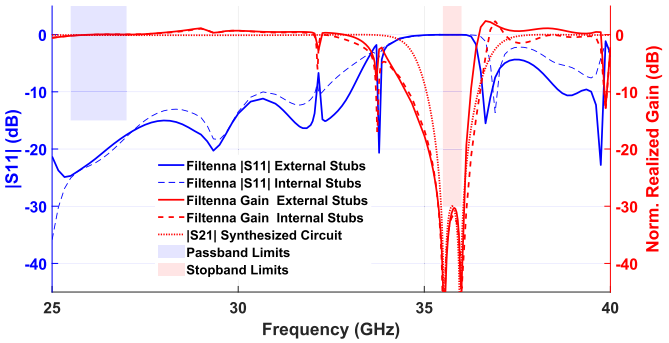

Fig. 8. $|S_{11}|$ and normalized broadside realized gain versus frequency of the coaxial horn filtenna. Gain curves are normalized to the gain at 26.5 GHz; at other frequencies thus the curves can exceed 0 dB due to the electrically larger aperture. Solid lines refer the design with the stubs in the horn profile, dashed lines refer the design with stubs in the coaxial profile.

at 26.25 GHz. The antenna matching in the passband is better than 18 dB for both designs. Also for both designs, the realized gain curve shows a flat behavior (within ±0.2 dB) in the passband range and nearly the expected 30 dB drop within the designated stopband frequency range. The peaks at 33.1 and 33.7 GHz are resonances of the lower Teflon ring, however they affect neither the passband nor the stopband. Fig. 9(a) shows the far-field characteristic of the designed filtenna, summarized as the superposition of the radiation patterns of the dominant left-hand circular polarization and its right-hand cross-polarization counterpart at 26.25 and 35.75 GHz.

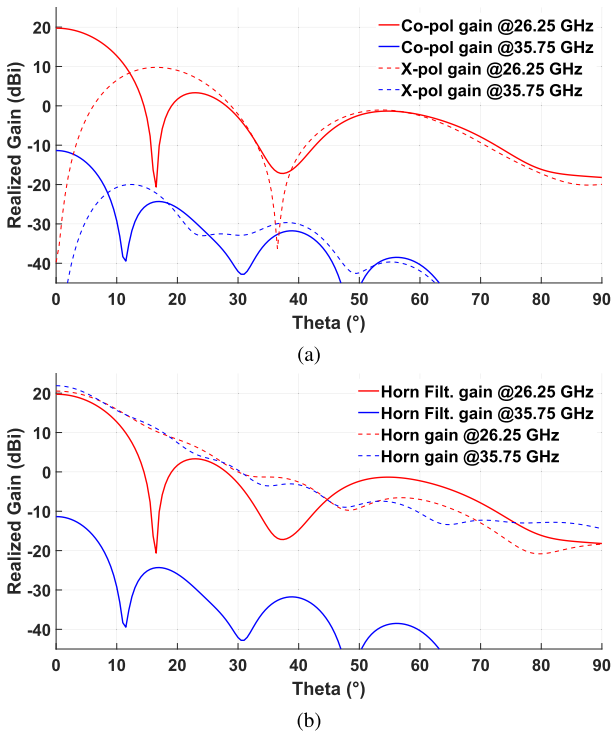

Fig. 9. Proposed horn filtenna exhibits more than 30 dB of overall radiation pattern attenuation between the passband and stopband, suppressing interference in any direction. (a) Co- and cross- polarized radiation pattern at passband and stopband. (b) Comparison between the designed horn filtenna and a standard horn (same outer size, nonfiltenna).

In the center of the passband, i.e., 26.25 GHz, the maximum gain is 19.6 dBi, while the half-power beamwidth is ±6.5° and within this angle, the axial ratio is lower than 3.5 dB. The gain suppression between the 35.75 GHz stopband curve and the 26.25 GHz passband one is on average more than 30 dB (neglecting radiation nulls). Fig. 9(b) shows instead the comparison of the designed coaxial horn filtenna with a standard horn antenna with similar dimensions. The gain of the filtenna is slightly penalized, compared to the 20 dB of gain of the horn in the passband due to the perturbation of the aperture introduced by the coaxial core (not by the IL of the filtering function). Instead, more than 30 dB of attenuation in the stopband is achieved, implying that the filtenna suppresses stopband radiation in every direction and thus reduces interference toward other onboard systems.

Simulations were first carried out using the ad hoc finite element method in a body-of-revolution formulation [17] and then further verified by the commercial software Ansys HFSS.

V. Manufacturing Considerations

Manufacturability of the designed coaxial filtenna involves as follows.

1) The outer horn: it can be assembled by stacking several laser-cut metal layers, a technique that can successfully applied up to 100 GHz. Alternatively, computer numerical control (CNC) lathing with inner-digging utensils can be used. The proposed solution with external stubs requires more advanced inner-digging capabilities.

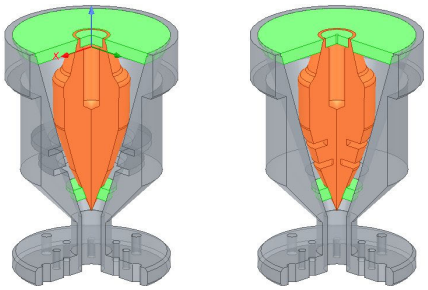

(a) (b)

Fig. 10. Sectioned 3-D view of the designed coaxial horn filtennas suitable for CNC lathing. In gray: metal horn. In orange: metal coaxial core. In green: Teflon rings. The hole in the top of the coaxial core is for CNC machinability only. (a) Stubs in the horn profile. (b) Stubs in the coaxial-core profile.

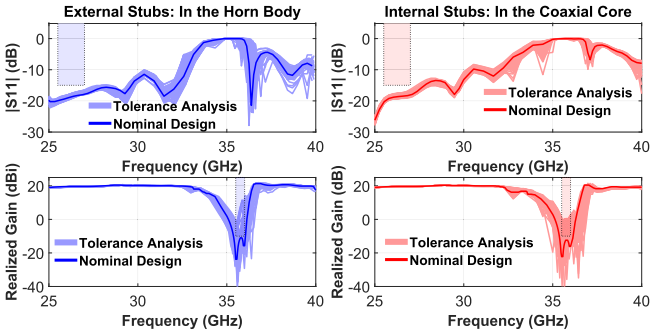

Fig. 11. Tolerance analysis of coaxial filters for CNC manufacturing. Each graph contains several curves corresponding to the simulations varying the filtenna physical dimensions with a normal distribution. The two top graphs correspond to the $|S_{11}|$, the bottom ones to the broadside gain. The right (red) graphs correspond to the filtenna with the stubs in the coaxial core. The left (blue) curves instead refer to the design with the stubs in the horn profile.

2) The coaxial core: it can be also manufactured by CNC lathing leveraging its full axial symmetry. Moreover, The hollow coaxial core can be 3-D printed or assembled from two parts to reduce the overall weight.
3) The Teflon rings: they may be manufactured by lathing and fit onto the coaxial structure. The innermost ring works as internal support, whereas the outermost works as a radome to avoid debris to enter the antenna. Specific surface processes are needed for space applications, however, this is not part of the scope of this work.

Ready-to-manufacture 3-D designs are shown in Fig. 10 for the two cases: external stubs (extending out of the horn body) or inner stubs (stubs carved into the coaxial core). For both designs, all the parts are compatible with CNC lathing. Some supports were made on the body of the horn to place the Teflon rings. Fig. 8 shows no electrical differences between the two designs. However, the tolerance analysis depicted in Fig. 11 shows that the design with the stubs in the coaxial-core profile is more tolerant to fabrication errors, particularly if one analyzes the stopband performance. This design also seems to be the best from a manufacturing point of view because it allows having a horn with a standard body, and all the complexity lies only in the metallic coaxial core.

The standard tolerance provided by commercial CNC fabricators for this design is ± 0.05 mm. To perform this analysis, it is assumed that all dimensions follow a normal distribution

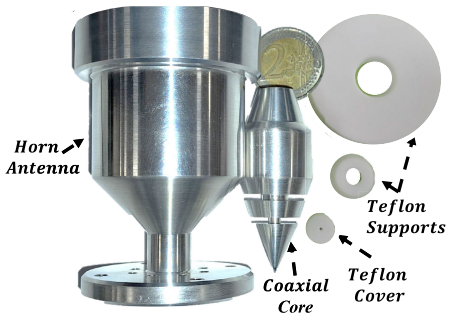

Fig. 12. Fabricated coaxial horn filtenna prototype. The prototype is composed of: a standard circular horn antenna, coaxial metal core with the dug resonant stubs, and Teflon supports. All these parts are assembled as shown in Fig. 10(b).

with the nominal value as the mean and ± 0.1 mm as three times the standard deviation. Furthermore, it is assumed that the coaxial core is not perfectly coaxial to the horn but has an inclination of up to $\pm 1^\circ$ with respect to the horn. Fig. 11 shows the tolerance analysis result. It is observed that there is almost no variation in the passband in any of the two designs; this was predictable since the filtenna is matched ($|S_{11}| > 10$ dB) in a wide bandwidth within this frequency range. On the other hand, the stopband behavior is more affected by manufacturing errors. It is also observed that the stopband behavior of the design with the stubs in the horn profile is more affected, with an attenuation better than 10 dB in the stopband in every random simulation, compared to that of the stubs in the coaxial core profile which always exhibits attenuation better than 20 dB within this frequency range. That is why a coaxial horn filtenna prototype with the stubs in the coaxial core is chosen for manufacturing.

VI. Manufactured Prototype and Results

The coaxial horn filtenna with the stubs carved into the coaxial core shown in Fig. 10(b) has been manufactured. All the blocks necessary for the operation of this filtenna prototype are shown in Fig. 12: standard circular horn antenna, metal coaxial core, and Teflon supports. All these parts are assembled accordingly and the measurement setup is described below. The filtenna is connected to a circular (d = 8.311 mm) to rectangular (WR28) waveguide transition, this, in turn, is connected to a WR28 to coaxial transition which is the one that is connected to the vector network analyzer Rohde & Schwarz ZVA50 through a coaxial cable. The measurements are de-embedded up to the WR28 waveguide section using through-reflect-line (TRL) calibration. The $|S_{11}|$ parameter is measured directly by the vector analyzer. Instead, a far-field measurement is performed to calculate the gain. A linearly polarized horn antenna with known gain and radiation pattern is used as a reference at one port and the device under test (DUT) at the other port. Knowing the distance between the antennas, the DUT gain can be estimated from the $|S_{21}|$. Note that under this setup it is only possible to measure linear polarization. However, circular polarization is known to be a linear combination of two perpendicular linear polarizations 90° degrees out of phase. Therefore, we measure in phase

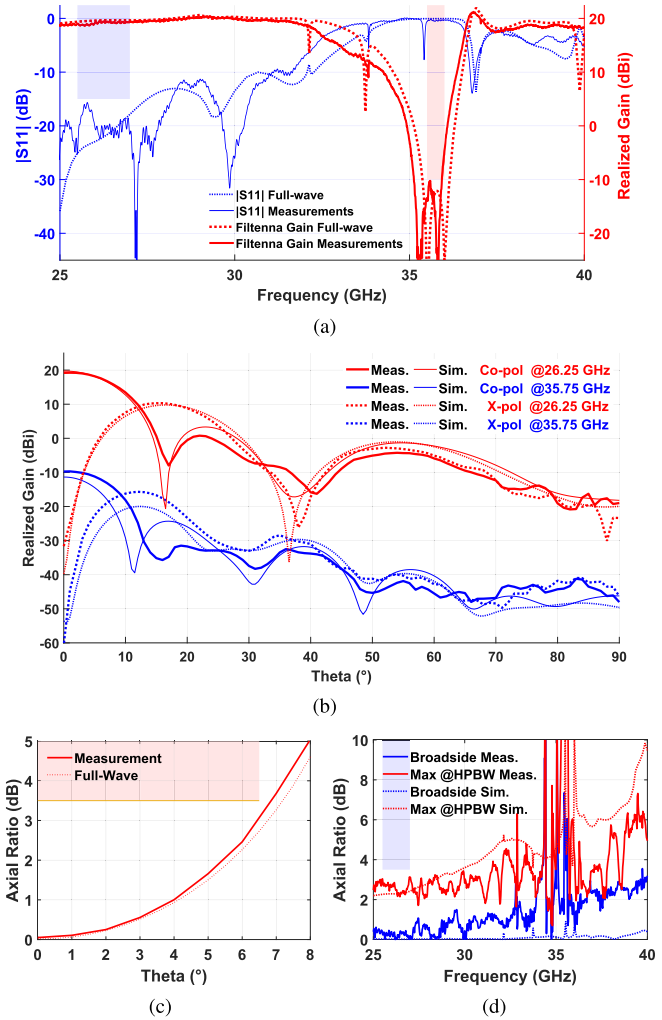

Fig. 13. Comparison between full-wave simulations (dotted lines) and measurements (solid lines) of coaxial horn filtenna with stubs in the coaxial core. Measured/simulated broadside gain @26 GHz: 19.2/19.6 dBi. (a) $|S_{11}|$ and Gain versus freq. (b) Radiation patterns at passband (26.25 GHz) and stopband (35.75 GHz). (c) Axial ratio versus angle at 26.5 GHz. (d) Axial ratio versus freq. The red lines are computed at broadside, the blue lines correspond to the maximum value within the HPBW.

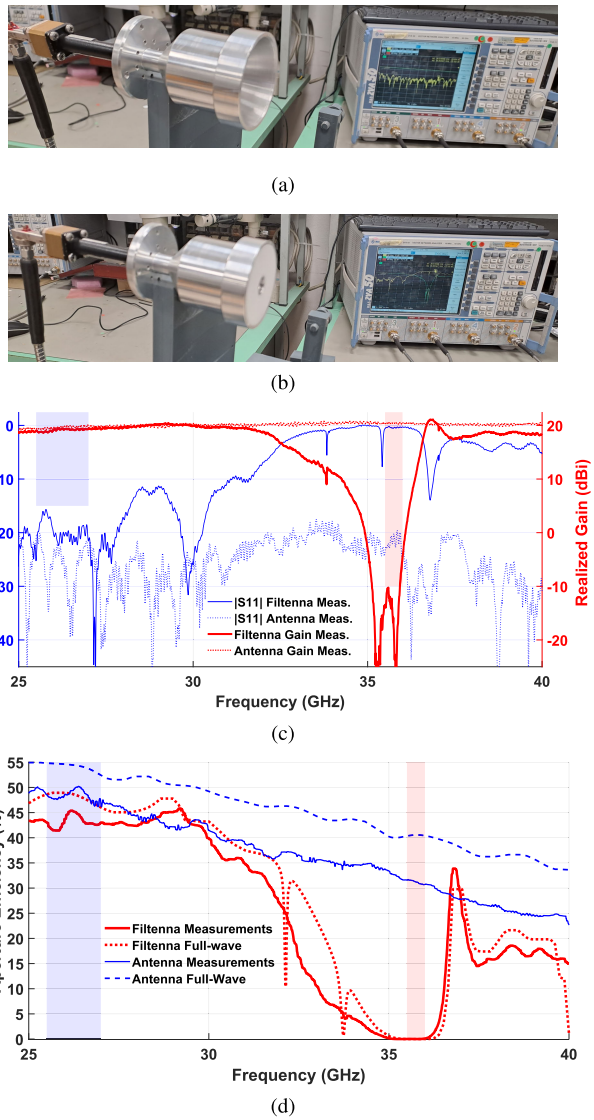

Fig. 14. Performance comparison between the standard horn and the filtenna. Measured filtenna/ standard horn antenna broadside gain at 26 GHz: 19.2/19.7 dBi. Measurement setup for (a) standard horn antenna, (b) coaxial horn filtenna (standard horn with the coaxial core inserted). (c) and (d) Comparison between the measurements of the coaxial horn filtenna and the standard horn.

and magnitude the two linearly polarized and orthogonal components G_H and G_V and with them we calculate the co-polar (RHCP) and cross-polar (LHCP) gain as well as the axial ratio as following:

$$G_{Copol} = (G_H + jG_V)/2, \quad G_{Xpol} = (G_H - jG_V)/2$$
$$AR = G_H/jG_V. \tag{4}$$

Fig. 13 shows a very good agreement between full-wave simulations and measurements. The measured filtenna broadside gain is 19.2 dBi in the passband and meets the specifications. The measured axial ratio is less than 3.5 dB within the half power beamwidth (±6.5°) across the entire passband, as shown in Fig. 13(c) and (d). Even though there is a slight frequency downshift of 150 MHz in the stopband (0.4% of the fractional bandwidth at 36 GHz), there is still more than 23 dB of attenuation across this entire band, exceeding the required minimum of 20 dB. The frequency downshift is partly because the stubs in the coaxial core were made about 0.1 mm larger than expected, but also because the Teflon mounts have kept the coaxial core in a higher position than it should be, so it protrudes slightly from the mouth of the horn antenna. This implies that the stubs are in a position where the horn flare is wider than projected, so its resonant frequency is lower than expected. The $|S_{11}|$ and gain spikes near to the stopband are present also in the full-wave simulations. Through the analysis of the electric and magnetic fields calculated by means of full wave simulations, it has been verified that these are resonances in the lower Teflon support. Through the measurements we have verified that the position in frequency and the amplitude of these peaks are slightly affected by the alignment and positioning of the coaxial core. Nonetheless, the passband remains clean. In this regard, it is stated that the pieces were assembled and held together only by the pressure exerted by the Teflon mounts toward the horn antenna.

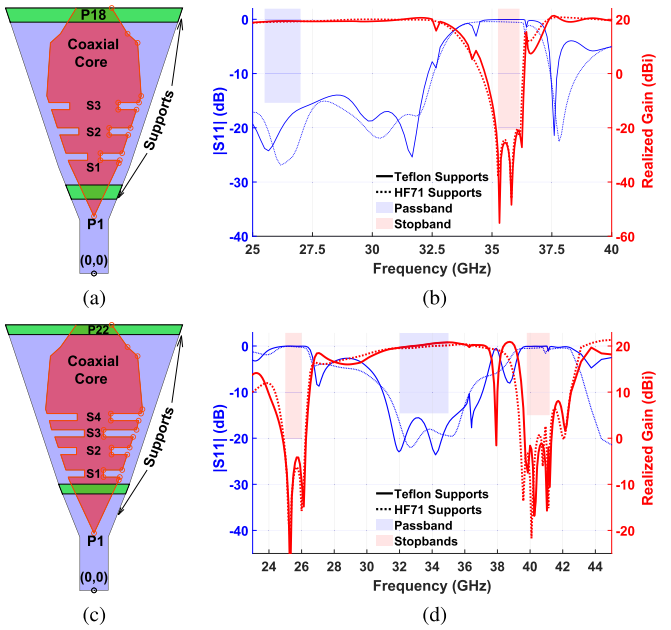

Fig. 15. Designs using the same antenna but different coaxial cores. (a) Coaxial designed to have 40 dB of attenuation within BW = 1 GHz: P = [(0,16.15), (7,31.15), (7.28,32), (1.81,32), (1.81,34), (7.95,34), (9.66, 39.14), (4.28,39.14), (4.28,41.14), (10.33,41.14), (12.00,46.28), (6.84,46.28), (6.84,48.28), (12.71,48.28), (13.33,50.16), (12.31,65.15) (9.47,67.73), (5,75)]. Support dimensions are the same as before. (b) Full-wave filtenna response of (a). (c) Coaxial designed to have two stopbands: P = [(0,16.15), (7,31.15), (7.28,32), (2.67,32), (2.67,34), (7.95, 34), (9.4,38.34), (4.94,38.34), (4.94,40.34), (10.06,40.34), (11.06,43.34), (2.73,43.34), (2.73,45.34), (12, 45.34), (12.6,47.94), (4.75,47.94), (4.75,49.94), (13.26,49.94), (13.67,51.16), (12.31,66.15), (9.47,68.73), (5,75)]. Teflon height is 3.25 mm. Lower Teflon support is located in Q4. (d) Full-wave filtenna response of (c). For (b) and (d) solid lines consider Teflon supports, dotted lines consider ROHACELL HF71 supports. The broadside gain is normalized to the value in the center passband: 19.2 dBi @26.25 GHz for (a) and (b), 20.4 dBi @33.5 GHz for (c) and (d); at other frequencies thus the curves can exceed 0 dB due to the electrically-larger aperture.

A performance comparison was also made between the standard horn antenna and the coaxial horn filtenna. The measurement setups for both cases are reported in Fig. 14(a) and 14(b), respectively. Fig. 14(c) shows the stopband filtering behavior of the filtenna in comparison with the flat gain across the entire frequency range of the horn antenna. Furthermore, the filtenna matching and gain are barely affected in the passband due to the insertion of the coaxial core ($\approx$ 0.5 dB of gain penalty). The simulated (measured) filtenna aperture efficiency is between 47 and 49 (41 and 45) % in the passband as shown in Fig. 14(d). This is comparable with the simulated (measured) efficiency of the standard conical horn antenna which is between 52 and 55 (46 and 50) % in the passband. Since the use case focuses on space applications, further studies on temperature stability, electrical breakdown points, and specific surface processes for space radiation are required. However, the initial step of validating the concept of inserting a filter function into a circular horn antenna without occupying more precious volume has been successfully completed. It might be speculated that any standard circular horn antenna could be converted into a filtenna simply by designing and inserting a suitable coaxial core with stubs, however, further study is required to establish possible constraints.

TABLE II
COMPARISON BETWEEN PROPOSED HORN FILTENNA WITH EXISTING DESIGNS

Ref.	Filtering Technique	Polarization Support	Performance (RL[dB], IL[dB], AT[dB])
[7]	Passband (PB), Screws	Linear	PB (RL>15, RL<0.2): 23.4 - 24.2 GHz. Stopband (AT>10): 21.4 - 22.5 GHz.
[8]	Passband, SIW FSS	Linear	PB (RL>15, IL<0.3): 9.75 - 11 GHz. Stopband (AT>10): 10.7 - 13 GHz.
[9]	Stopband, SSR Array	Linear	PB (RL>15, IL<1.5): 7.5 - 9.3 GHz. Stopband (AT>35): 9.7 - 9.9 GHz.
[10]	Stopband, SSR Array	Linear	PB (RL>15 , IL<0.3): 11 - 12 GHz. Stopband1 (AT>5): 9.0 - 9.2 GHz Stopband2 (AT>5): 10.3 - 10.6 GHz.
[11]	Dualband, SRR	Circular	PB1(RL>15,IL<0.1):13.2–14.1GHz. PB2 (RL>15,IL<0.1):16.3–17.1GHz. Stopband (RL<2.5): 15 - 16 GHz.
This work	**Stopband, Coaxial Radial Stubs**	**Linear, Dual Linear, Circular**	Manufactured use-case design: PB (RL>15, IL<0.5): 25 - 30 GHz. Stopband (AT>30): 35.3 - 35.9 GHz. Simulated additional design 1: PB (RL>15, IL<0.9): 25 - 30 GHz. Stopband (AT>40): 35.2 - 36.2 GHz. Simulated additional design 2: PB (RL>15, IL<0.9): 32 - 35 GHz. Stopband1 (AT>20): 24.9 - 26 GHz. Stopband2 (AT>15): 39.7- 41.2 GHz.

VII. ADDITIONAL DESIGNS WITH STUBS CARVED INTO THE COAXIAL CORE

Two additional coaxial cores have been designed in order to demonstrate that different filtering functions can be implemented in a given standard horn antenna by inserting different coaxial cores with the resonant stubs carved on it. The first one intends to improve the stopband performance of the use-case design by inserting an additional stub as shown in Fig. 15(a). Therefore, a three-TZs response is obtained. This improves the stopband attenuation from 30 to 40 dB and the stopband bandwidth form 600 MHz to 1 GHz as show in Fig. 15(b). The second one is a dual stopband design. It requires 15 dB of RL in the passband: 32–35 GHz. The two stopbands are centered at 25.5 and 40.5 GHz with 1.1 and 1.5 GHz of bandwidth, respectively. The required stopband attenuation are 20 and 15 dB, respectively. The lower stopband is implemented using the TM_{120} mode of the stubs S3 and S4 of Fig. 15(c). The TM_{130} mode of these stubs resonate right in the upper stopband. These resonances together with the TM_{120} mode of the stubs S1 and S2 implement the fourth-order behavior in the upper stopband as shown in Fig. 15(d). Please note in the solid lines of Fig. 15(b) and (d) that the bottom Teflon resonates and adds undesired spikes. These resonances are at 32.5 GHz, 33.5 GHz for the single stopband design and at 36 GHz, 38 GHz for the dual stopband one. They are out of the bands of interest, therefore, they are not such a problem. However, the air-like material ROHACELL HF71 ($\varepsilon_r = 1.093$) can be used instead of Teflon so that these spikes do not appear as shown in the dotted lines of Fig. 15.

VIII. COMPARISON WITH EXISTING DESIGNS

Table II shows a comparison between the presented work with horn filtenna designs existing in the literature. The

presented coaxial horn antenna supports linear, dual linear, and circular polarization. This is an advantage over the previous works that only one of them supports. Furthermore, the presented work is the best compromise between stopband attenuation and passband IL. The works in [7], [8], [10], and [11] presented a lower in-band IL, however its stopband behavior is far from the one presented here. On the other hand, the work in [9] has a comparable stopband attenuation (AT) performance, however, its IL is higher. This difference is because in [9] the stopband resonators are made in a naturally lossy substrate while in the presented work they are air-filled.

IX. Conclusion

This article proposes an innovative concept to approach radio frequency interference mitigation in space missions. The concept is based on the integration of filtering functions in the downlink antenna which offers a space-efficient way of improving isolation by suppressing out-of-band emissions. A synthesis and design method for filtennas has been introduced and extensively described targeting circular horns. The paradigm can address several practical use-cases with a clear advantage in radio frequency interference management. In-line coaxial radial stubs allow to realize complex low-loss filtering functions and perfectly fit circular symmetry along horn antennas, thus compatible with circular polarization. This concept can be applied to a standard horn antenna and converted into a filtenna by inserting a suitable coaxial core that implements the required filtering function. A Ka-band coaxial horn filtenna has been designed and manufactured and the measurements fit the simulated results.

References

[1] R. D. Leach and M. B. Alexander, "Electronic systems failures and anomalies attributed to electromagnetic interference," NASA Marshall Space Flight Center MSFC, Huntsville, AL, USA, NASA STI/Recon Tech. Rep. N, Jul. 1995, p. 16608.

[2] *Electrical and Electronic Engineering*, Standard ECSS-E-ST-20, European Cooperation for Space Standardization, Noordwijk, The Netherlands, Oct. 2019.

[3] *Electromagnetic Compatibility*, Standard ECSS-E-ST-20-07C, European Cooperation for Space Standardization, Noordwijk, The Netherlands, Feb. 2012.

[4] *Electromagnetic Compatibility*, Standard ECSS-E-HB-20-07A, European Cooperation for Space Standardization, Noordwijk, The Netherlands, Sep. 2012.

[5] *Radio Frequency and Modulation*, Standard ECSS-E-ST-50-05C Rev. 2, European Cooperation for Space Standardization, Noordwijk, The Netherlands, Oct. 2011.

[6] L. Gourdeau et al., "Altimetry in a regional tropical sea [space agencies]," *IEEE Geosci. Remote Sens. Mag.*, vol. 5, no. 3, pp. 44–52, Sep. 2017.

[7] A. A. C. Alves, L. G. da Silva, E. C. V. Boas, D. H. Spadoti, and A. S. Cerqueira, "Mechanically tunable horn filtenna for mm-waves," in *Proc. 13th Eur. Conf. Antennas Propag. (EuCAP)*, Mar. 2019, pp. 1–4.

[8] G. Q. Luo et al., "Filtenna consisting of horn antenna and substrate integrated waveguide cavity FSS," *IEEE Trans. Antennas Propag.*, vol. 55, no. 1, pp. 92–98, Jan. 2007.

[9] S. S. Roy, C. Saha, N. K. Mallenahalli, and D. Sarkar, "Circular split ring resonator (C-SRR) array integrated frequency-notched horn-filtenna with wide and strong rejection band," *IEEE Access*, vol. 9, pp. 52664–52671, 2021.

[10] M. Barbuto, F. Trotta, F. Bilotti, and A. Toscano, "Horn antennas with integrated notch filters," *IEEE Trans. Antennas Propag.*, vol. 63, no. 2, pp. 781–785, Feb. 2015.

[11] M. Barbuto, F. Trotta, F. Bilotti, and A. Toscano, "Design and experimental validation of dual-band circularly polarised horn filtenna," *Electron. Lett.*, vol. 53, no. 10, pp. 641–642, May 2017. [Online]. Available: https://ietresearch.onlinelibrary.wiley.com/doi/abs/10.1049/el.2017.0145

[12] M. Oldoni, S. C. Mejllones, S. C. Mejillones, S. Moscato, and A. Giannini, "Ka-band coaxial horn filtenna for enhanced electromagnetic compatibility on spacecraft," in *Proc. IEEE MTT-S Int. Microw. Filter Workshop (IMFW)*, Nov. 2021, pp. 269–271.

[13] M. Oldoni, S. C. Mejillones, S. Moscato, and A. Giannini, "Filtennas in space: A novel approach for radio-frequency interference mitigation," in *Proc. ESA Workshop Aerosp. EMC (Aerospace EMC)*, May 2022, pp. 1–6.

[14] J. Bornemann and S. Y. Yu, "Novel designs of polarization-preserving circular waveguide filters," *Int. J. Microw. Wireless Technol.*, vol. 2, no. 6, pp. 531–536, Dec. 2010.

[15] D. Pozar, *Microwave Engineering*, 4th ed. Hoboken, NJ, USA: Wiley, 2011.

[16] S. C. Mejillones, M. Oldoni, S. Moscato, G. Macchiarella, M. D'Amico, and G. G. Gentili, "Accurate synthesis of extracted-pole filters by topology transformations," *IEEE Microw. Wireless Compon. Lett.*, vol. 31, no. 1, pp. 13–16, Jan. 2021.

[17] G. G. Gentili, P. Bolli, R. Nesti, G. Pelosi, and L. Toso, "High-order FEM mode matching analysis of circular horns with rotationally symmetric dielectrics," *IEEE Trans. Antennas Propag.*, vol. 55, no. 10, pp. 2915–2918, Oct. 2007.

Steven Caicedo Mejillones received the bachelor's degree in telematics engineering and the master's degree in telecommunications from the Escuela Superior Politécnica del Litoral (ESPOL), Guayaquil, Ecuador, in 2014 and 2017, respectively, and the Ph.D. degree in information technology from the Politecnico di Milano, Milan, Italy, in 2023.

From 2014 to 2018, he worked as a Planning and Optimization Engineer for radio access networks (RAN) in different telecom companies in Ecuador, like the mobile operator Claro from América Móvil Group, Mexico. From 2018 to 2021, he was an early-stage Researcher at SIAE Microelettronica, Milan, within the H2020 Marie-Curie ITN 5G STEP FWD Program. Since 2021, he has been a Microwave Designer for space, backhaul, and O-RAN applications at SIAE. His research interests include synthesis and design techniques for microwave filters, filtering antennas, and phased array antennas.

Matteo Oldoni (Member, IEEE) was born in Milan, Italy, in 1984. He received the Ph.D. degree in information technology from the Politecnico di Milano, Milan, in 2013.

He has worked as a Microwave Designer at the Passive Microwave Components Laboratory, SIAE Microelettronica, Cologno Monzese, Italy, becoming a Member of Technical Staff, and cooperated with several companies and research institutions internationally. Since June 2022, he is a full-time Researcher at the Electronics, Information and Bioengineering Department, Politecnico di Milano. His research interests include synthesis and design techniques for microwave filters, algorithms development for computer-aided tuning, and antenna design.

Mr. Oldoni was a recipient of the Young Engineers Prize of the 39th European Microwave Conference.

Stefano Moscato (Student Member, IEEE) was born in Pavia, Italy, in 1988. He received the Ph.D. degree in electronics engineering from the University of Pavia, Pavia, in 2016.

He was a visiting Ph.D. student at Georgia Tech, Atlanta, GA, USA, in early 2015. He became part of the Research and Development Microwave Group, SIAE Microelettronica, Cologno Monzese, Italy, in May 2017. From September 2022, he is the Head of the 1337 Research and Development Group devoted to the design and validation of mm-wave passive components, antennas and sub-systems. He is involved in innovation programs and founded researches for microwave backhauling, O-RAN equipment, and space-oriented assemblies. He is the author of more than 40 papers on international journals and conferences. His research activities have been focused on RF-to-mm-wave passive component.

Dr. Moscato was a recipient of the IEEE MTTS Undergraduate/Pre-Graduate Scholarship in 2012. He was the Chair of the IEEE Student Branch, University of Pavia, from 2013 to 2016.

Michele D'Amico (Senior Member, IEEE) received the master's degree from the Politecnico di Milano, Milan, Italy, in 1990, and the Ph.D. degree in mathematics from the University of Essex, Essex, U.K., in 1997.

Since 2002, he has been an Associate Professor in applied electromagnetics at the DEIB, Politecnico di Milano. He has several patents on antennas and has authored or coauthored more than 130 papers published in international journals or conference proceedings. Since May 2013, he has been responsible for the experimental activities of the Spino d'Adda Laboratory, Politecnico di Milano, dedicated to the experimental investigation of EM waves in the troposphere. His research interests include antennas, electromagnetic wave propagation in the troposphere at frequencies above 10 GHz, and radarmeteorology.

Gian Guido Gentili received the Laurea degree in electronics engineering from the Politecnico di Milano, Milan, Italy, in 1987.

He was a Visiting Scholar at Universidad Politécnica de Madrid, Madrid, Spain, in 1993 and 1995. He joined as a Researcher with the Dipartimento di Elettronica ed Informazione, National Research Council (CNR), Center for Space Telecommunications, Politecnico di Milano, in 1989. In 2001, he became a Senior CNR Researcher. He became an Associate Professor with the Politecnico di Milano, in 2002. He is responsible for the Electromagnetics Laboratory, Politecnico di Milano "Wavelab". His research interests include numerical method for electromagnetics (finite elements, method of moments, and mode-matching), antennas and feed systems for terrestrial and space applications, microwave passive devices, microwave filter analysis, and design and plasmonics.

Open Access funding provided by 'Politecnico di Milano' within the CRUI CARE Agreement